Numerical Tours

Constant Bourdrez
Master IASD

January 15, 2025

1 Linear Programming

1.1 Optimal Transport of Distributions

We begin with the following dataset, which represents a heart with random points within a small region:

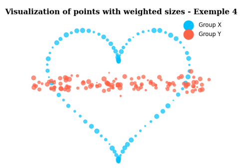

Figure 1: Dataset visualization.

This configuration leads to the transport plan shown in fig. 2a, along with the optimal coupling connection as depicted in fig. 2b.

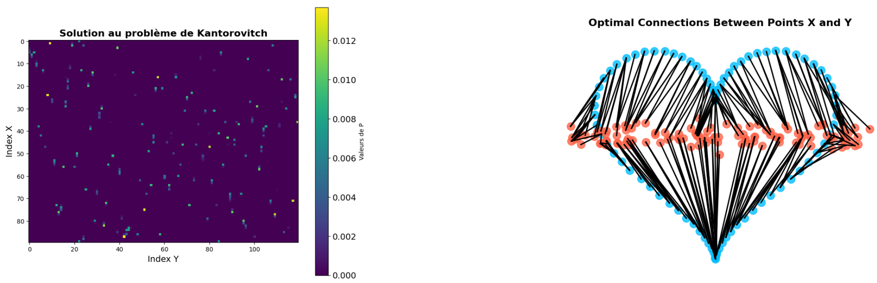

(a) Transport plan.

(b) Optimal coupling.

Figure 2: Transport and optimal coupling results.

1.2 Displacement Interpolation

From the optimal transport plan $\mathbf{P}^\star$, we compute the W_2-geodesic path $(\mu_t)_t$, which is defined as:

$$\mu_t = \sum_{i,j} \mathbf{P}^\star_{i,j} \delta_{(1-t)x_i + ty_j}$$

Applying this to our dataset, we obtain the barycenter distributions shown in fig. 3:

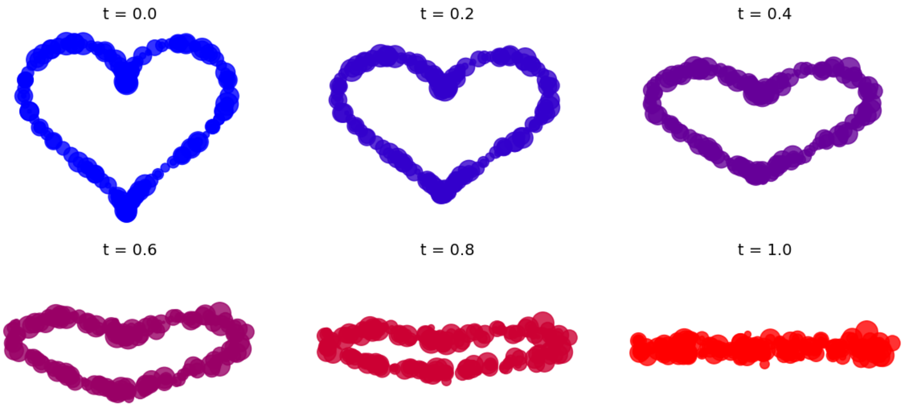

Figure 3: Barycenter distributions.

1.3 Optimal Assignment

In this variation of the dataset, the optimal transport plan becomes a permutation matrix $\mathbf{P}^\star = P_{\sigma^\star}$, and the heatmap of this matrix is shown in fig. 4a, where two distinct colors are used to represent the plan.

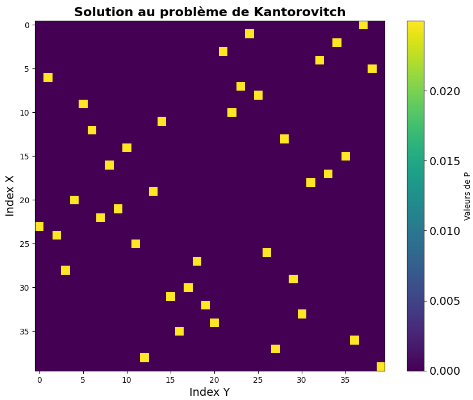

(a) Optimal transport plan $\mathbf{P}^\star$.

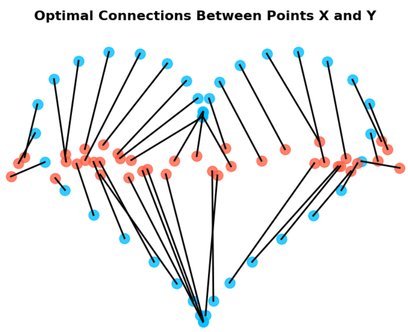

(b) Optimal assignment $x_i = y_{\sigma^\star(j)}$.

Figure 4: Optimal assignment process.

2 Entropic Regularization of Optimal Transport

2.1 Transport Between Point Clouds

Exercise 1. We consider the following point cloud data:

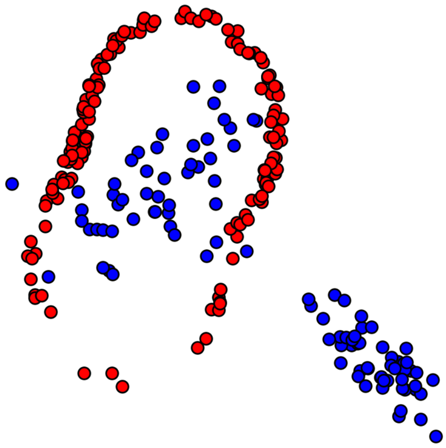

Figure 5: Point cloud visualization.

The optimal transport plan reveals a notable structure, as seen in the following results.

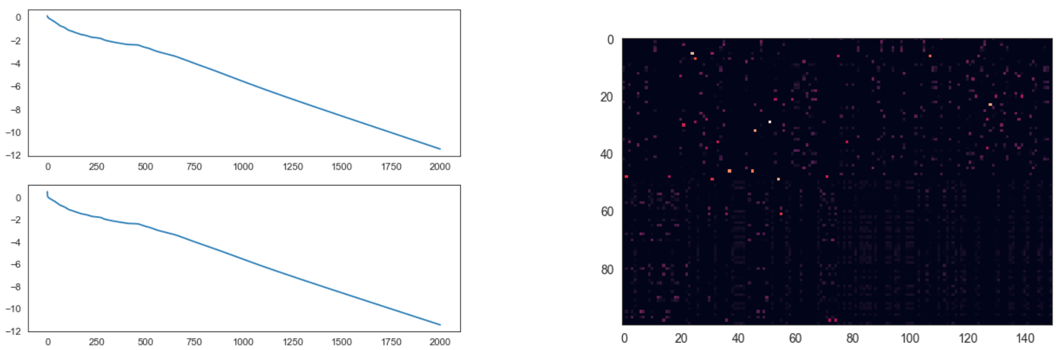

(a) Convergence of the L^1 error on the marginals.

(b) Optimal transport plan.

Figure 6: Convergence and optimal transport plan for regularization strength $\varepsilon = 0.01$.

We derive the following relation for the computation of the L^1 error:

$$P^{(l+1)}\mathbb{1} = \operatorname{diag} u^{(l+1)} K v^{(l+1)} = \frac{a}{Kv^{()}} \odot K v^{(l+1)}$$

which facilitates efficient calculation of the error.

Exercise 2. We compute the regularized optimal transport for various values of $\varepsilon \in \{0.002, 0.004, 0.005, 0.01, 0.1, 0.3\}$, as shown below:

The smallest value tested without encountering underflow is $\varepsilon_{\min} = 1.10^{-2}$.

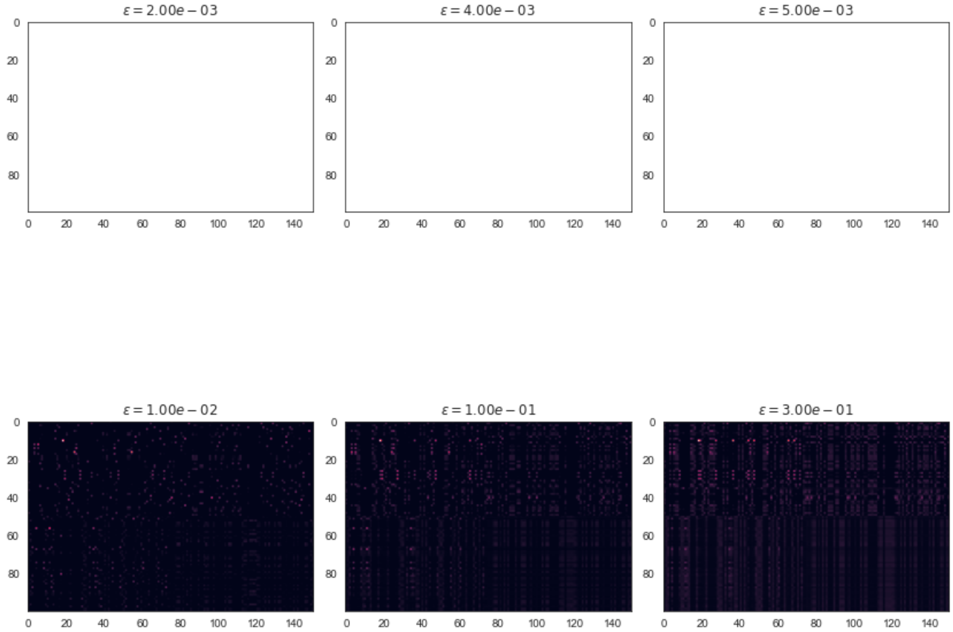

Figure 7: Optimal transport plans for varying ε.

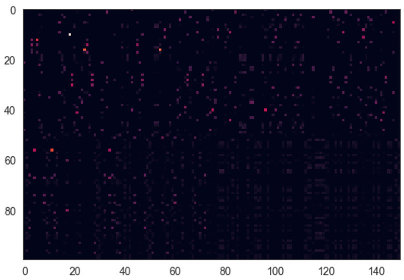

(a) Optimal transport plan $\mathbf{P}^\star_\varepsilon$.

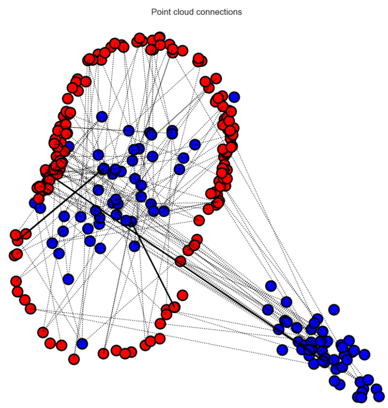

(b) Point cloud connections for $\varepsilon = 1.10^{-2}$.

Figure 8: Transport plans and connections.

2.2 Transport Between Histograms

We work with the following data, where the marginals are a mixture of Gaussian and Laplace distributions, as shown in fig. 9. The unnormalized functions are given by:

$$\begin{aligned} f_1(x) &= \exp\left(-\frac{(x-1/2)^2}{2\sigma^2}\right) + 0.6\exp\left(-\frac{(x-0.65)^2}{2\sigma^2}\right) \\ f_2(x) &= 0.4\exp\left(-\frac{|x-0.2|}{\beta}\right) + 0.6\exp\left(-\frac{|x-0.8|}{\beta}\right) \end{aligned} \tag{2.1}$$

Exercise 3. We use the regularization strength $\varepsilon = (0.03)^2$. The optimal coupling and transport map are given figs. 10a and 10b.

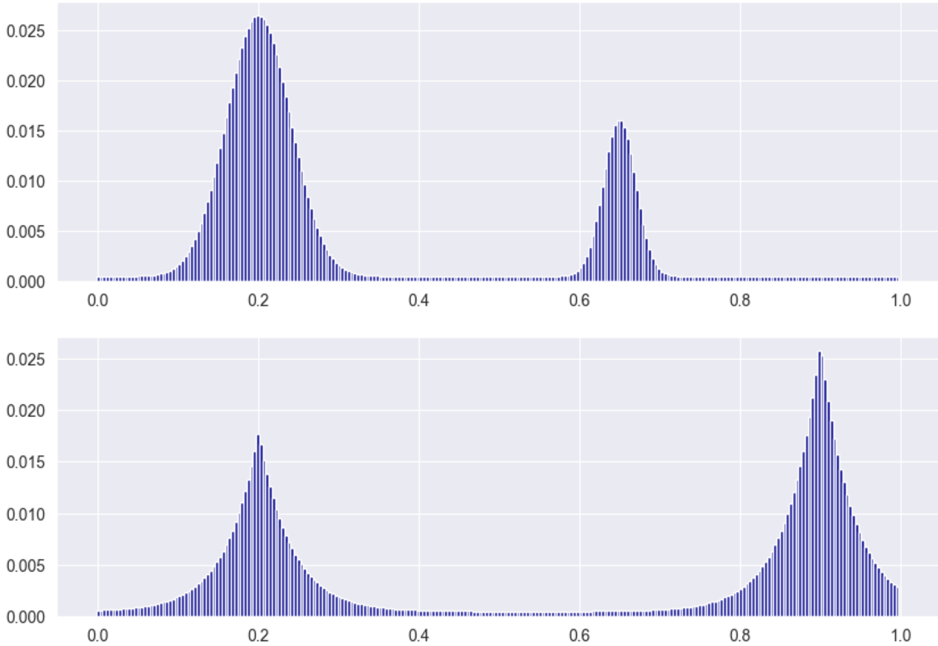

Figure 9: Histograms of the marginal distributions.

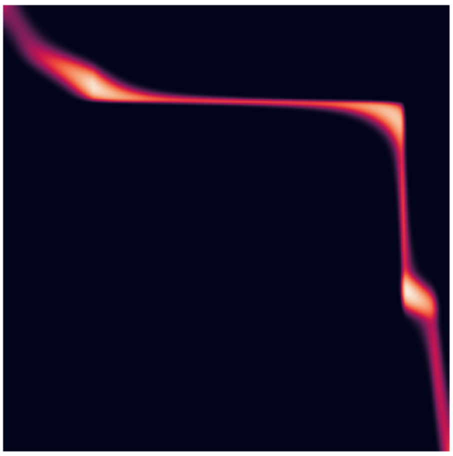

(a) Optimal coupling between the histograms.

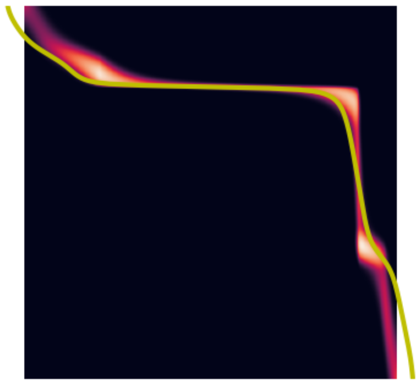

(b) Associated transport map.

Figure 10: Coupling and transport map for $\varepsilon = (0.03)^2$.

Bonus exercise. Figure 11 shows the coupling and transport map for a lower regularization strength ε.

2.3 Wasserstein barycenters

We use the data fig. 12 and regularization parameter $\varepsilon = (0.04)^2$.

Exercise 4. Figure 13 shows the result.

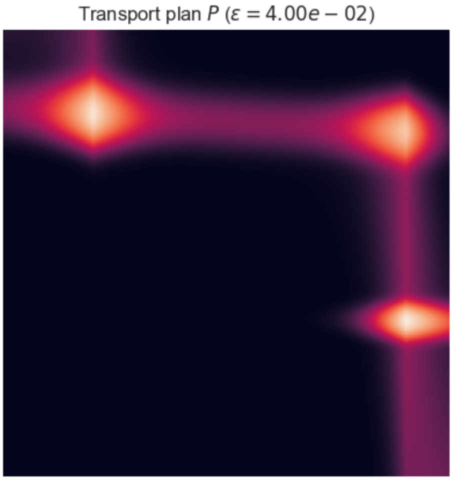

(a) Optimal coupling between the histograms.

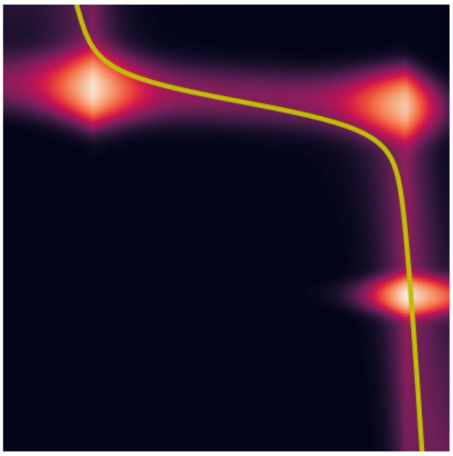

(b) Associated transport map.

Figure 11: Coupling and transport map for $\varepsilon = (0.03)^2$.

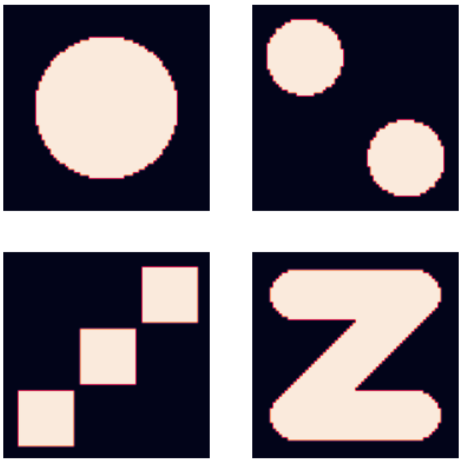

Figure 12: Bitmap image data.

Exercise 5. We compute Wasserstein barycenters for bilinear interpolation weights $t, s \in \{0, 0.25, 0.5, 0.75, 1.0\}$ – see fig. 14.

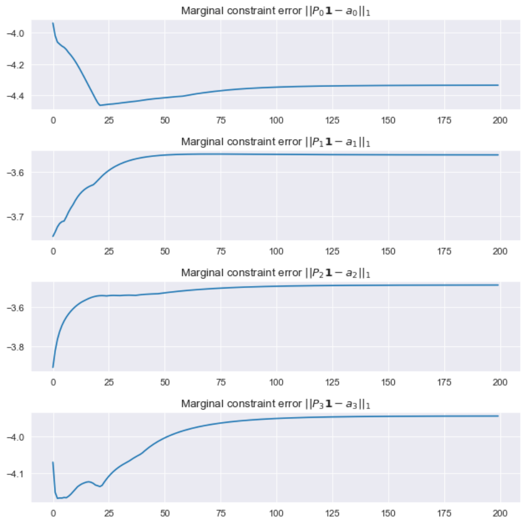

(a)

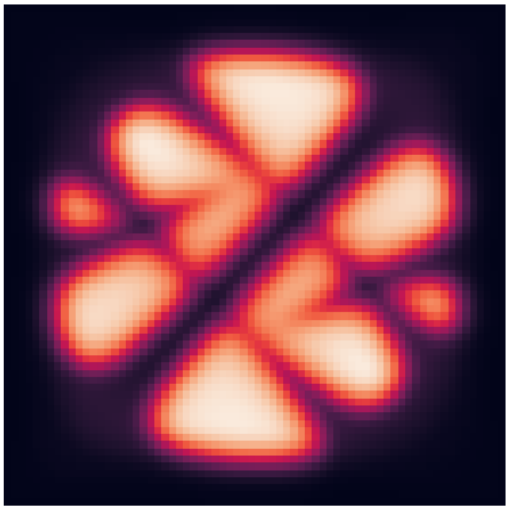

(b)

Figure 13: Convergence and result of the Bregman algorithm to compute the Wasserstein barycenters of the images in fig. 12.

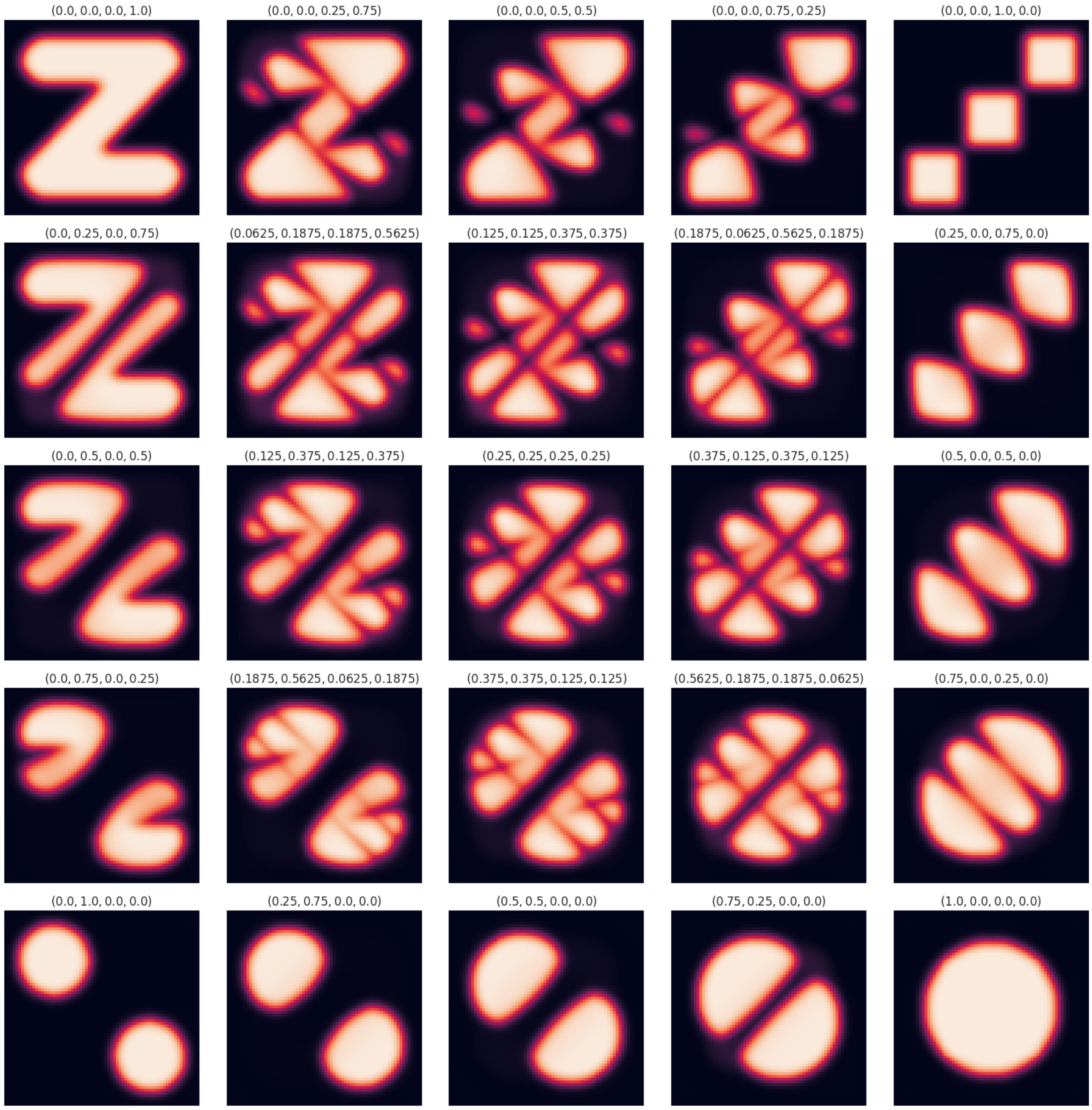

Figure 14: Set of Wasserstein barycenters.